since 1961

Age assessment of the Jasmund Glacitectonic Complex (SW Baltic Sea) by quartz luminescence dating of syn-kinematic deposits

Nikolas Krauß, Michael Kenzler, Heiko Hüneke*

Abstract. The development of the Fennoscandian Ice Sheet (FIS) in its SW Baltic Sea sector during MIS 2 led to the formation of the Jasmund Glacitectonic Complex (JGC). The evolutional stages of the latter reflect small-dimensioned ice sheet oscillations. A glacitectonically formed piggyback basin is in focus to give direct information on the evolution of the JGC. We present a set of five OSL ages from syn-kinematic glacilacustrine and alluvial fan sediments deposited between ice margin-parallel thrust-bounded ridges from the southern margin of the JGC. The ice front proximal depositional environment and short transport distances of the sediments implicate a possible insufficient bleaching of the luminescence signal. Nonetheless, we were able to gain reliable ages of ~22 ka for the growth of the southern JGC. The samples pre-date the Oder ice stream reaching its maximum extent, the Pomeranian ice marginal belt at ~18–20 ka. A comparison of our data with the existing age data related to the evolution of the JGC will contribute to a better understanding of the FIS dynamics in the research area and the timing of the Pomeranian phase in NE Germany.

*Nikolas Krauß** (*nikolas.krauss@uni-greifswald.de*), ⓘ *https://orcid.org/0000-0003-2573-1777*
*Michael Kenzler (*kenzlerm@uni-greifswald.de*), ⓘ *https://orcid.org/0000-0003-3754-1495*
*Heiko Hüneke (*hueneke@uni-greifswald.de*), ⓘ *https://orcid.org/0000-0001-7509-8768*
University of Greifswald, Institute of Geography and Geology, Greifswald, Germany
**Corresponding author*

INTRODUCTION

During the Weichselian (~115–11.7 ka; Litt *et al.* 2007; Cohen *et al.* 2013) repeating advances of the Fennoscandian Ice Sheet (FIS) shaped the morphology of the SW Baltic Sea area. Many questions regarding the maximum extent of ice marginal belts (IMB) and their timing are still under discussion (Hughes *et al.* 2016; Lüthgens *et al.* 2020; Kleman *et al.* 2021). From the last decade on, publications progressively describe an asynchronous extent of the FIS in this area (Houmark-Nielsen 2010; Marks 2012; Lüthgens *et al.* 2020; Tylmann *et al.* 2022).

Advances of the FIS lead to the development of several glacitectonic complexes in its SW periphery (Van der Wateren 1986; Pedersen 2005, 2014; Pedersen, Gravesen 2009; Gehrmann 2018; Gehrmann,

Harding 2018, 2019). As glacitectonic complexes originate from proglacial deformation, they are not only scale models for orogenic deformation, they furthermore permit an insight into regional ice sheet evolution (Pedersen 2005). Glacitectonic deformation displays regional ice dynamics and palaeoenvironmental conditions (Pedersen 2005; Gehrmann 2018; Gehrmann, Harding 2018; Winsemann *et al.* 2020). Winsemann *et al.* (2020) pointed out that glacitectonic complexes provide the potential to determine the extent of glaciers and ice sheets during a specific time, whilst also providing information on ice marginal dynamics and the interaction of an ice-sheet with its foreland.

One of the largest glacitectonically deformed landscapes in the SW Baltic Sea region is the Jasmund Glacitectonic Complex (JGC) (Figs 1A, B; Groth 2003;

Ludwig 2011; Gehrmann 2018; Gehrmann, Harding 2018, 2019; Gehrmann *et al.* 2017, 2022) on the island of Rügen. A multiphase evolutional model that integrated all parts of the complex was suggested by several authors (Groth 2003; Ludwig 2011; Gehrmann 2018; Gehrmann, Harding 2018, 2019; Gehrmann *et al.* 2022). Common in all the mentioned models is a two-step main evolution, leading to the development of the northern and the southern sub-complex (Fig. 1B). Gehrmann *et al.* (2022) deciphered the principal structural evolution with the formation of the northern before the southern sub-complex based on morphological and structural features. The stratigraphic interpretation of the JGC formation is mainly based on lithostratigraphic constraints and isolated dating results (Panzig 1995; Niedermeyer *et al.* 2010; Kenzler *et al.* 2015, 2017, 2022, 2023). Gaining numerical age data bears some difficulties due to the lack of directly dateable material. For temporal reconstruction of such complexes, sediments are required that were deposited during their formation.

In order to get new insight into the chronologic evolution of the JGC we present a set of five new OSL ages from syn-kinematic siliciclastic deposits of glacilacustrine and alluvial origin. We test the deposits in order to gain robust age data on the development of the JGC. Corresponding with the fact that an ice advance formed the JGC (Kenzler *et al.* 2022), we aim to pre-date an ice marginal position by the evolution of a glacitectonic complex. In addition, we integrate the dating results in a cross-regional scale to test the latest models on the dynamics of the FIS during the late Weichselian.

Regional setting and lithostratigraphic units

The Jasmund peninsula as a part of the island of Rügen is located in the SW Baltic Sea in the NE part of Germany (Fig. 1A). At several cliff outcrops along the coastline of the Jasmund peninsula, the glacitectonically thrusted and folded strata of the JGC are easily accessible. The glacitectonic framework shows strong similarity to the glacitectonic deformation structures visible at the Upper Cretaceous chalk cliffs of Møns Klint in SE Denmark (Pedersen, Gravesen 2006, 2009; Aber, Ber 2011). Credner (1893) already recognized that the morphology of the Jasmund peninsula is dominated by subparallel ridges striking in different main directions (Fig. 1B). Keilhack (1912) and Jaekel (1917) were the first subdividing the structural setting of the typical depositional succession of the JGC, which consists of glacitectonically imbricated blocks of Upper Cretaceous (Maastrichtian) chalk, paraconformably overlain by Pleistocene deposits (Fig. 2). The latter represent a succession of three diamictons interpreted as till units (M0, M1 and M2; Jaekel 1917; Panzig 1995) representing Elsterian (~400–320 ka; Litt *et al.* 2007) or late Saalian (~191–126 ka; Cohen, Gibbard 2011) and Weichselian ice advances of the FIS. The stratigraphic classification of the particular till layers was determined by fine-gravel analysis and correlation with the regional Quaternary stratigraphy in the SW Baltic Sea area (Panzig 1995) as well as luminescence dating (Krebetschek 1995; Panzig 1995; Kenzler *et al.* 2015, 2017, 2022, 2023) and a few radiocarbon ages (Steinich 1992). These tills are partially interbedded by units of (gla-
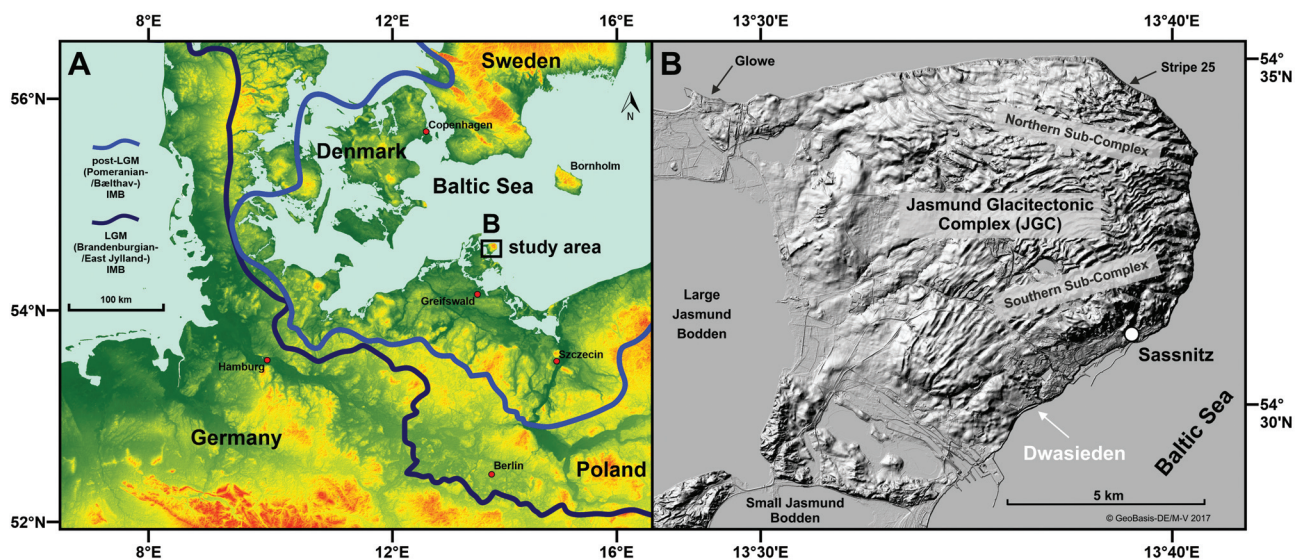
Fig. 1 A – Map of the SW Baltic Sea region with Last Glacial Maximum (LGM, Brandenburgian/East Jylland phase, early MIS 2) and post-LGM (Pomeranian/Bælthav phase, MIS 2) ice marginal belts based on Ehlers *et al.* (2011) and Houmark-Nielsen (2010). Black rectangle shows the study area, the Jasmund peninsula, as a part of the island of Rügen. B – Digital Elevation Model (DEM5, 10 times exaggerated, hill shade; processed by J. Hartleib) of the Jasmund peninsula showing the Jasmund Glacitectonic Complex (JGC) divided into the northern and the southern sub-complex, the study site Dwasieden and other important cliff sections mentioned in the text (Kenzler *et al.* 2022, 2023)

ci-)fluvial and (glaci-)lacustrine sediments (I1 and I2) representing (inter-)stadial units deposited under ice-free conditions (Kenzler, Hüneke 2019). A fourth till unit M3 (Jaekel 1917; Panzig 1995) is disconformably overlying the older deposits.

The oldest glacial deposit to be discovered on the Jasmund peninsula is the M0 diamict. It intermittently overlies the Maastrichtian chalk and is discussed to be deposited by an Elsterian (MIS 10; Panzig 1995; Litt *et al.* 2007) or Saalian advance of the FIS (Drenthe phase, MIS 8/6; Niedermeyer *et al.* 2010; Kenzler *et al.* 2017). The overlying M1 unit is deposited by a late Saalian ice advance (Warthe phase, MIS 6; Litt *et al.* 2007). The following lithostratigraphical unit I1 consists of mostly silty and sandy (inter-)stadial sediments with layers of fine-grained gravel at the base (Fig. 2; Panzig 1995; Kenzler *et al.* 2022, 2023).

The M2 till represents an early MIS 2 (LGM, Brandenburgian/Frankfurt phase) advance of the FIS. It is overlain by the predominantly silty and sandy I2 unit.

Forming the top section of the outcrop, the M3 till displays a MIS 2 re-advance of the late Weichselian (post-LGM, Pomeranian/Mecklenburgian phase, Niedermeyer *et al.* 2010; Kenzler *et al.* 2010, 2017). At the base of the M3 complex, the main glacitectonic angular unconformity (GAU, Kenzler *et al.* 2023) is located, separating the whole sequence in pre- (plus locally syn-) and post-kinematic glacitectonic strata (Fig. 2). The strata closely associated with the GAU
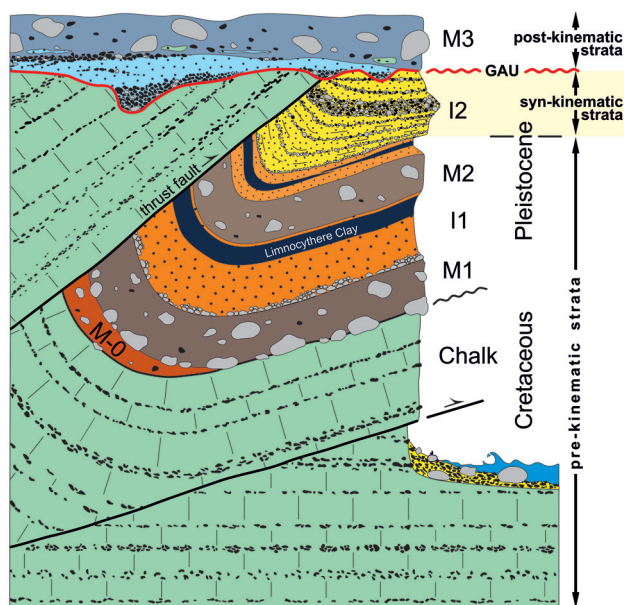
Fig. 2 Tectonostratigraphic section of the Jasmund peninsula (modified from Kenzler *et al.* 2023), including syn-kinematic strata of the upper I2 unit as a key feature of the glacitectonic imbrication on the Jasmund peninsula (Plonka *et al.* 2022; Kenzler *et al.* 2023). Undulated red line shows the glacitectonic angular unconformity (GAU) at the base of the M3 unit

can be seen as a key to the chronological interpretation, as it has been deposited immediately before (respectively, during) or immediately after the formation of the JGC.

In particular, the detection of syn-kinematic deposits as a part of the I2 unit offers the potential to directly date the evolution of the JGC and give insight into the dynamics of the FIS at the same time (Kenzler *et al.* 2023). These syn-kinematic strata were recently identified at the southern sub-complex (Plonka *et al.* 2022) and the northern sub-complex (Kenzler *et al.* 2023).

Up to now, geochronological data in connection with the evolution of the JGC (nearly without exceptions) refers to pre-kinematic strata (Steinich 1992; Krbetschek 1995; Panzig 1995; Kenzler *et al.* 2015, 2017, 2022; Pisarska-Jamroży *et al.* 2018a).To date the evolutional stages of the JGC, sediments are required to be deposited simultaneously to the development. A depositional environment revealing these syn-kinematic deposits is found in piggyback basins. Piggyback basins are not only a common feature of thrust belts, in smaller scale they also develop in glacitectonic complexes during thrust-fault deformation between thrust-bounded ridges (Pedersen 2005, 2014; Plonka *et al.* 2022; Kenzler *et al.* 2023). Piggyback deposits discovered in glacitectonic complexes thereby reflect the development of glacitectonic deformation.

At the southern boundary of the JGC, the nearly 300 m long active cliff section of Dwasieden has recently been in focus of numerous studies (Fig. 1B). Previous works focused on the polyphase deformation of the Pleistocene tills on the basis of microstructural investigation (Brumme 2015; Brumme *et al.* 2019). Pisarska-Jamroży *et al.* (2018a, 2019) identified soft-sediment deformation structures (SSDS) in late Weichselian glacilacustrine and glacifluvial deposits as evidence for glaci-isostatically induced crustal faulting. Furthermore, ice-rafted debris (IRD) of (overturning) ice rafts in a local Weichselian proglacial lake were described (Pisarska-Jamroży *et al.* 2018b).

As a part of the Dwasieden cliff, Plonka *et al.* (2022) identified a sedimentary succession implicating the evolution of a piggyback basin. They described the syn-kinematic basin filling during the second evolutional stage of the JGC (growth of the southern sub-complex), providing a detailed study on the stepwise evolution of the basin based on sedimentological analyses. The synoptic sedimentary log of the piggyback basin filling displays the growth stages during the formation of the JGC (Fig. 3). The log illustrates the upper part of the synoptic lithostratigraphic section of the Jasmund peninsula (Fig. 2, lithostratigraphical units M2-I2-M3). The focus is on
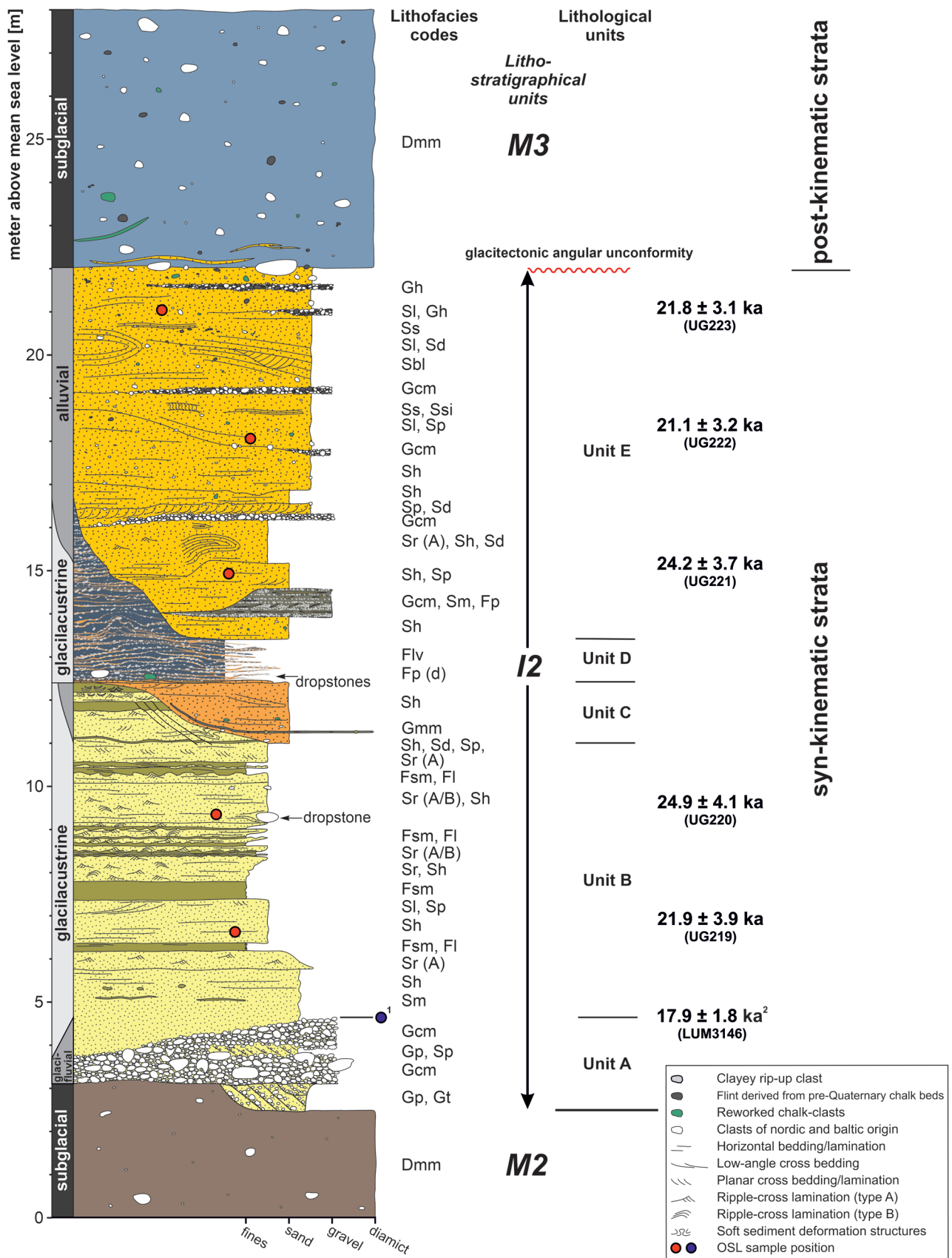
Fig. 3 Synoptic lithological log of the Dwasieden cliff section showing information about sedimentary features, lithostratigraphic units and OSL age classification (modified after Plonka *et al.* 2022). Red dots show OSL sample position of the presented study. Facies codes are adopted from Miall (1996) and Benn, Evans (2010). [1] Sample position and [2] OSL age are from Pisarska-Jamroży *et al.* (2018a)

the I2 unit, which can be subdivided into five lithological units referred to as A to E from bottom to top (Fig. 3; Plonka *et al.* 2022).

Unit A is directly overlying the M2 till and reaches up to 3.5 m in thickness, thinning out towards SW. It is dominated by two beds of boulder-rich sandy gravel, intercalated by cross-bedded gravelly sand. Unit A is mainly deposited by high-rate meltwater discharge from the proximal glacier front, with intercalated sand indicating a phase of less energetic flow. The contact to the underlying M2 till is sharp and locally truncating due to erosional channels in dm scale.

Unit B is up to 9.2 m thick and consists of fine- to medium-grained parallel- and cross-laminated sand intercalated by cm- to dm-scaled silt beds. The deposits of unit B are thinning out towards NE. An outsized clast within a bed of horizontally laminated sand is interpreted as a dropstone (Fig. 3). The sediments display a glacilacustrine phase with meltwater influx and alternating sedimentation from suspension and from bed load in the form of hypo- and hyperpycnal flows. Polyvalent palaeo-current directions indicate several meltwater sources into the lake.

Unit C consists of medium- to coarse-grained sand with occasional gravel beds and a cm-scaled diamictic bed in the lower part. With a maximum 1.4 m thickness, it marks the filling of a local erosional channel. This unit documents the drainage of the proglacial lake, due to changes in the geomorphological setting.

Unit D is composed of rhythmically alternating layers of fine-grained sand, silt and clay in which rip-up clasts of clay are abundant. It is up to 5.8 m thick and is thinning out towards SW. This unit displays a phase of recurring accumulation of meltwater deposits in the basin and the continued development of a proglacial lake.

The uppermost unit E consists mainly of medium- to coarse-grained sand generally coarsening upwards. Towards the top of the up to 8.6 m thick unit, occasional gravel beds appear. An up to 1 m thick pebble bed at the base, mostly consisting of the rip-up clasts of unit D, indicates the local erosion of the underlying unit. A broad range of sedimentary structures indicates the depositional environment to be more high-energetic than observed in the former units. This unit documents a setting of alluvial and fan delta progradation into the basin. The boundary between unit E and the overlying M3 till is the GAU described above.

This part of the Dwasieden cliff section offers the potential to directly date the development of the JGC. To test if the sediments described in Plonka *et al.* (2022) reveal the potential to gain robust OSL ages, this work presents a set of five new OSL ages from syn-kinematic deposits of the lithostratigraphical I2 unit (MIS 2), located at the margin of the southern sub-complex of the JGC.

METHODS

Methods – luminescence dating

Luminescence dating on proglacial sediments offers a possibility to date the development of glacial landforms which are directly related to ice margins and thereby used to reconstruct the extent of ice advances. An advantage of luminescence dating is the abundance of quartz and feldspar mineral grains that are ubiquitous in glacial deposits rather than e.g. organic material for radiocarbon dating. The effect of incomplete bleaching of sample material, as a result of insufficient sunlight exposure, on age calculation is a general issue. This can be circumvented by measuring samples on (quasi-) single-grain level and the application of statistical models (Galbraith *et al.* 1999; Fuchs, Owen 2008; Thrasher *et al.* 2009).

Methods – luminescence sample preparation

For luminescence dating, five samples (UG219-223) were retrieved by using an opaque PVC liner or stainless steel tins. Samples were taken from glacilacustrine and alluvial deposits of the units B and E (Fig. 3). Preparation and equivalent dose (D_e) measurements were conducted at the luminescence lab of the University of Greifswald under subdued red light. Samples were dry sieved to obtain the coarse-grained fraction of 100–150 μm. A standard cleaning and separation technique followed. To remove carbonates and dispersion of aggregates, the samples were treated with HCl and sodium oxalate ($Na_2C_2O_4$). H_2O_2 was used to remove organic matter. Quartz mineral fractions were separated using sodium polytungstate solution. The last step in preparing was the etching of quartz grains with 40% HF for 40 minutes to exclude feldspar contamination and affection of alpha radiation on the outer rim of quartz grains, followed by the dissolution of fluorides using 20% HCl and the final wet sieving step.

Following the single aliquot regenerative-dose measurement protocol (Table 1, SAR; Murray, Wintle 2000) using quasi single-grain aliquots (equivalent to < 1 mm aliquots), the OSL signal was measured by using a Risø TL/OSL DA-20 reader equipped with a ^{90}Sr/^{90}Y beta source (Bøtter-Jensen *et al.* 2010). To determine the most suitable preheat temperature, several test measurements were conducted on medium aliquots (6 mm). The test measurements (Fig. 4), such as preheat plateau, dose recovery and thermal transfer test, were conducted on sample UG222. The test results recommended a preheat temperature of 240°C and a cutheat temperature of 220°C. This is in conformity with test results gained from glacifluvial sediments of similar provenance published in Kenzler *et al.* (2022, 2023).

According to Wintle and Murray (2006), recuperation < 5% of the natural signal was applied as a rejection criterion, whereas the recycling ratio was set at 15%. Studies on OSL dating of partly bleached (glacifluvial) sediments yielded robust results working with this rejection criteria (Hardt *et al.* 2016). To exclude a possible feldspar contamination, an additional IRSL measurement at the end of each SAR sequence was conducted, in which an IR depletion ratio of > 0.9 was applied (Duller 2003).

The OSL decay curve displays a fast decreasing OSL signal within the first second, exhibiting a fast component domination (Fig. 5). For the isolation of the fast component OSL signal from the medium and slow ones, an early-background subtraction was used (Cunningham, Wallinga 2010). Therefore, the background integral (0.48–1.6 s) was subtracted from the integral of the first 0.48 s.

Plonka *et al.* (2022) describe a fast changing depositional environment proximal to the glacier front for the strata under investigation. Hence, insufficient bleaching, as addressed for glacifluvial sediments in e.g. Fuchs and Owen (2008) and Lüthgens *et al.* (2010a), has to be considered for the sample material dated in this study. Reasons for that exist in the depositional environment proximal to the glacier front, short transport distances and suspension load (Plonka *et al.* 2022). This might lead to an overestimation of depositional ages because of an unknown residual signal which adds to the OSL signal accumulated since the last transport event (Fuchs, Owen 2008; Arnold *et al.* 2009; Thrasher *et al.* 2009).

Previous works on samples from glacifluvial deposits (Fuchs, Owen 2008; Thrasher *et al.* 2009; Hardt *et al.* 2016; Lüthgens *et al.* 2010a, b, 2011a, b) focus on single-grain or quasi single-grain measurements to obtain robust depositional ages. Cunningham and Wallinga (2012) have shown that both types of measurements are suitable for dating of partially bleached sediment. To minimize the effect of insufficient bleaching on the obtained D_e values, in this work an analysis on quasi single-grain niveau (Murray *et al.* 2012; Hardt *et al.* 2016) was chosen as a preferable option. Duller (2008) pointed out that it is common that 90–95% of the emitted luminescence signal is derived from 5–10% of the grains or less. Tests on Weichselian glacifluvial sediments from NE Germany on single-grain niveau have shown that only 3–5% of quartz grains emit a significant luminescence signal (Lüthgens *et al.* 2010b, 2020; Hardt *et al.* 2016). Hence, reducing the number of quartz grains on an aliquot to a small amount should provide a luminescence signal derived from only one grain. In this work the grains on each accepted < 1 mm aliquot were counted to determine the average grain number, which is a more precise method than calculating the average

Table 1 Single aliquot regenerative dose protocol (SAR) used to determine the equivalent-dose of quartz mineral grains in this study

Run	Treatment
1	Dose (except before first run)
2	Preheat (240°C for 10 s)
3	Optical stimulation with IR-diodes for 100 s at 125°C (only for last run)
4	Optical stimulation with blue LEDs for 40 s at 125°C
5	Give test dose
6	Cut heat at 220°C
7	Optical stimulation with blue LEDs for 40 s at 125°C
8	Return to run 1
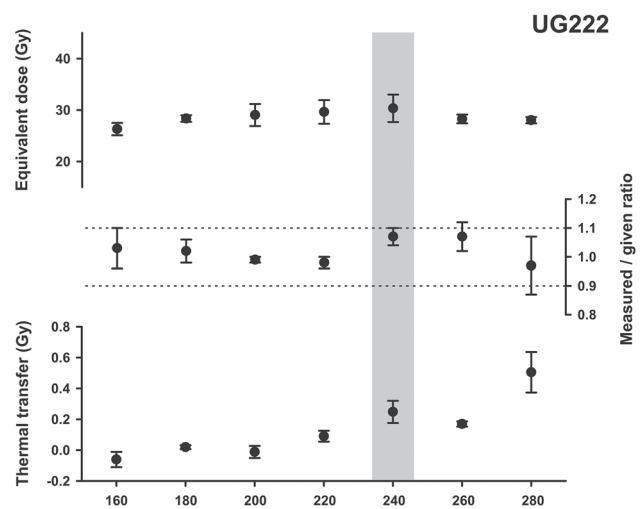
Fig. 4 Results of OSL test measurements (preheat plateau, dose recovery and thermal transfer) depending on preheat temperatures from 160–280°C. Each data point represents the mean value of three measured 6 mm aliquots. Shaded column displays chosen preheat temperature (240°C) for the SAR protocol used
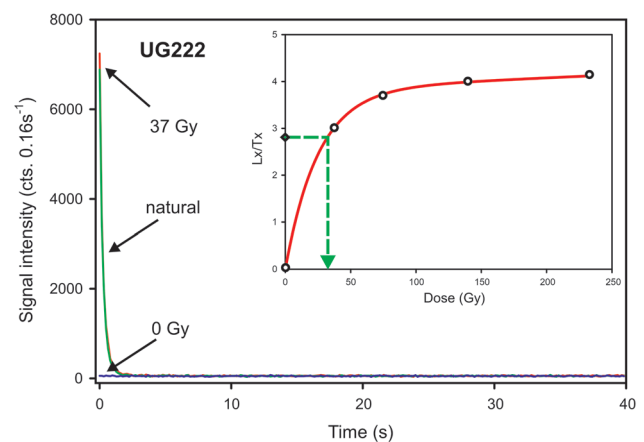
Fig. 5 OSL-signal decay curve for representative sample UG222, showing natural (green), 0 Gy (blue) and 37 Gy (red) dosed signal. Growth curve (red) and plotted natural signal (dashed green) are shown in the inserted box

number of grains. Grain numbers on a single aliquot range between 26 (UG221) and 33 (UG220) (Table 3). For comparison, the average number of grains for 1 mm aliquots was calculated using R studio and the Luminescence Package (Kreutzer et al. 2020). Based on a mean grain size of 125 µm and a packing density of 0.65, the calculated grain number for an aliquot results in 42, which is significantly higher.

To obtain reproducible age estimates, at least 50 equivalent dose (D_e) values (Rodnight 2008) have to pass the rejection criteria (Table 3). Following the investigation of Rodnight (2008) for determination of the burial dose, the Minimum Age Model (MAM, Galbraith et al. 1999) was chosen.

Methods – dose rate determination

For sediment dose-rate determination, the concentrations of uranium (U), thorium (Th) and potassium (K) were analyzed using low-level gamma spectrometry at VKTA e.V. (Dresden). The conversion factors of Guérin et al. (2011) were used to calculate the external dose-rate. According to Prescott and Stephan (1982) and Prescott and Hutton (1994), the contribution of cosmic radiation to the environmental dose was estimated as a function of geomagnetic latitude, altitude and burial depth of the samples.

The in-situ water content was determined, whereas the saturated water conten was calculated with cylindrical volumeters for each sample (Kenzler et al. 2017). The in-situ water content ranges between 2.6 and 4.1%, the determined water saturation ranges between 24.7 and 26.3% (Table 2). An increased water content attenuates the absorption of radiation by the sediment and thereby lowers the dose rate. As palaeohydrological conditions differ strongly from present-day conditions, the water content for the samples over burial time can only be estimated. The development of the piggyback basin described in Plonka et al. (2022) suggests changing water content of the pore space in the sediment. Another influence on the water content is the tilting of the strata due to glacitectonic deformation. Furthermore, the groundwater level has changed during the last ~10 ka due to the development of the Baltic Sea and glaci-isostatic rebound (Andrén et al. 2011). In order to take these factors of uncertainty into account, an average water content of 10 ± 8% is assumed for the calculation of the dose rate. This provides a possibility to cover a broad range between minimum and maximum water content, but results in higher absolute errors regarding the calculated ages. The radionuclide concentrations and the calculated dose rates are shown in Table 2.

Table 2 General sample information and summary of results from radionuclide analyses, water content determination and total dose rate

| Sample ID | Altitude (m a.s.l.)[a] | Depth below ground (m)[a] | Grain size (µm) | Potassium (%) | Thorium[b] (ppm) | Uranium[c] (ppm) | Water content (%) | | | Total dose rate (Gy ka^{-1}) |
							in situ	saturated	for age calculation	
UG223	17	6	100–150	1.13 ± 0.08	2.56 ± 0.20	1.09 ± 0.22	2.7	24.7	10 ± 8	1.60 ± 0.16
UG222	4	19	100–150	0.94 ± 0.08	1.79 ± 0.14	0.57 ± 0.11	2.6	26.1	10 ± 8	1.10 ± 0.15
UG221	4	19	100–150	1.03 ± 0.08	1.94 ± 0.16	0.6 ± 0.16	3.0	26.3	10 ± 8	1.19 ± 0.15
UG220	8	15	100–150	0.96 ± 0.08	2.06 ± 0.16	0.87 ± 0.20	4.1	25.7	10 ± 8	1.20 ± 0.15
UG219	5	18	100–150	0.69 ± 0.06	1.42 ± 0.12	0.6 ± 0.12	3.8	25.1	10 ± 8	0.86 ± 0.13

[a] Values display the height a. s. l/depth below ground in the field and do not correlate with sample position in the synoptic lithological log (Fig. 3); [b] Thorium concentration was calculated from the actvities of ^{228}Ac, ^{208}Tl and ^{212}Pb; [c] Uranium concentration was calculated from the actvities of ^{214}Pb and ^{214}Bi

Table 3 Results of OSL measurements and age calculation

Sample ID	Aliquot size	No. of aliquots[a]	Avg. grain number	Over dispersion (%)	Mean D_e (Gy)	MAM D_e(Gy)	MAM age (ka)
UG223	1 mm	52 (480)	30	32.0	41.7 ± 2.3	32.3 ± 2.9	21.8 ± 3.1
UG222	1 mm	53 (528)	28	17.9	28.5 ± 1.0	23.1 ± 1.7	21.1 ± 3.2
UG221	1 mm	51 (576)	26	28.9	37.5 ± 2.0	28.9 ± 2.4	24.2 ± 3.7
UG220	1 mm	50 (288)	33	33.4	38.8 ± 2.8	29.9 ± 3.1	24.9 ± 4.1
UG219	1 mm	50 (480)	28	30.8	27.9 ± 1.4	18.8 ± 1.6	21.9 ± 3.9

[a]Aliquots that passed rejection criteria (total number of measured aliquots)

RESULTS

Results – quartz luminescence measurements

A summary of the luminescence measurements is shown in Table 3. The calculated ages are ranging between 21.1 ± 3.2 ka (UG222) and 24.9 ± 4.1 ka (UG220). Taking the overlapping errors into account, the ages are stratigraphically consistent.

The distribution of D_e values for two representative samples (UG221 and UG223) is shown in Fig. 6. Both samples display a broad distribution of D_e values and exhibit a positive skewness in D_e distribution of 1.8 (UG221) and 1.5 (UG223). Skewness towards the smaller D_e values indicates a luminescence signal which is at least partly emitted by insufficiently bleached mineral grains (Fuchs *et al.* 2007; Fuchs, Owen 2008). The overdispersion, which indicates the spread of D_e values, ranges between comparatively low 17.9 % (UG222) and 33.4 % (UG220). Deposits from ice marginal areas tend to exhibit comparatively high overdispersion values due to different bleaching characteristics of mineral grains resulting in the spread of D_e values (Lüthgens *et al.* 2010b; Hardt *et al.* 2016). To determinate the true burial dose of a sample, different statistical age models can be applied (Galbraith *et al.* 1999; Olley *et al.* 1999; Roberts *et al.* 2000; Lepper, McKeever 2002). For samples from a proglacial depositional environment, it is recommended to apply the Minimum Age Model (MAM, Galbraith *et al.* 1999). The MAM allows to correct insufficiently bleached aliquots from D_e analysis by the setting of sigma_b (σ_b), as a parameter of overdispersion expected for a well-bleached sample from the dataset (Cunningham, Wallinga 2012). Shen *et al.* (2015) used $\sigma_b = 0.1$ (e.g. 10 % overdispersion) as a characteristic value for their quartz samples from flood deposits regarded as well-bleached. As a standard value for single-grain data, $\sigma_b = 0.2$ (e.g. 20% overdispersion) could be applied as a realistic esti-

mation (Arnold, Roberts 2009). For multi-grain data, σ_b must be smaller due to averaging in grain-to-grain variation (Cunningham *et al.* 2011; Cunningham, Wallinga 2012). Cunningham *et al.* (2011) show overdispersion depending on the number of grains per aliquot. In this study, $\sigma_b = 0.15$ was chosen for the presented data set (Table 3).

Results – reliability of the OSL data

The valid application of the SAR protocol (Murray, Wintle 2000) was approved by dose recovery tests in each SAR sequence. Additional IRSL measurements at the end of each SAR sequence (Table 1) were carried out to exclude possible feldspar contamination (Duller 2003). As the palaeohydrological conditions can only be estimated, uncertainties regarding the water content were displayed by a comparatively high overall error of ± 8%. According to the investigations of Cunningham *et al.* (2011) and the overdispersion values ascertained for the dataset at hand, the setting of $\sigma_b = 0.15$ is regarded as adequate.

Figure 7 shows an abanico plot of the calculated ages. The univariate plot displaying the kernel density estimate (KDE) shows a clear bimodal distribution. For samples UG220 und UG221 displaying ages around 24 ± 4 and 25 ± 4 ka, a residual luminescence signal of the penultimate deposition cycle cannot fully be excluded. The samples are from glacilacustrine and alluvial deposits. The dropstone in unit B (UG220) implicates an ice-contact glacial lake, which is accompanied by meltwater supply and suspension load. Slumps and slides from the basin margin additionally might lead to redeposition of sediments and hence to a mixture of grains with different bleaching intensities. Slumps and slides may also be a cause for insufficient resetting of the luminescence signal for parts of unit E (UG221). For this unit, Plonka *et al.* (2022) describe a higher-energetic depositional environment compared to the previous units with abundant meltwater
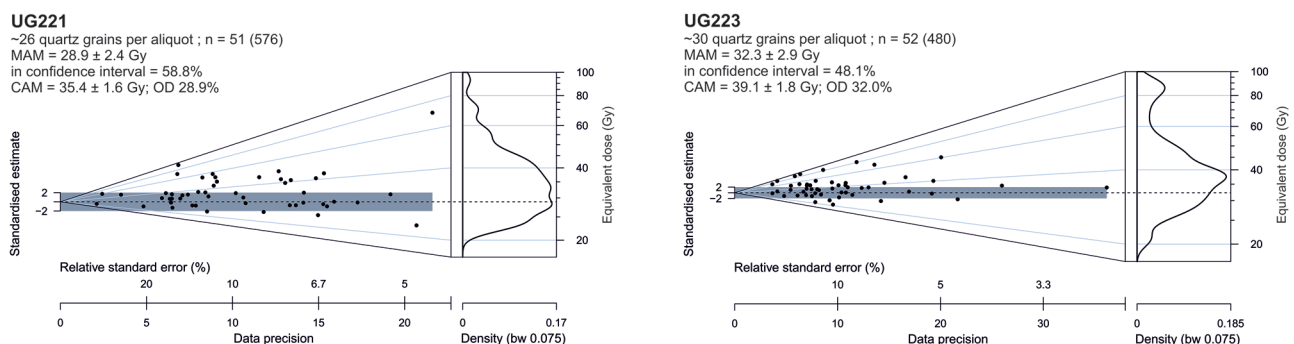
Fig. 6 Abanico plots showing the D_e distributions of representative samples UG221 and UG223. D_e values are shown on a log-scale. Dark grey horizontal bar (dispersion bar) displays the 2σ range around the dashed central value line (centrality line) defined as the MAM. N = number of aliquots that passed the rejection criteria, in brackets: total of aliquots measured per sample

OSL age distribution

UG219-223: n = 5 | mean age = 22.8 ± 3.6 ka
UG219, 222, 223: n = 3 | mean age = 21.6 ± 3.4 ka
UG220, 221: n = 2 | mean age = 24.6 ± 3.9 ka
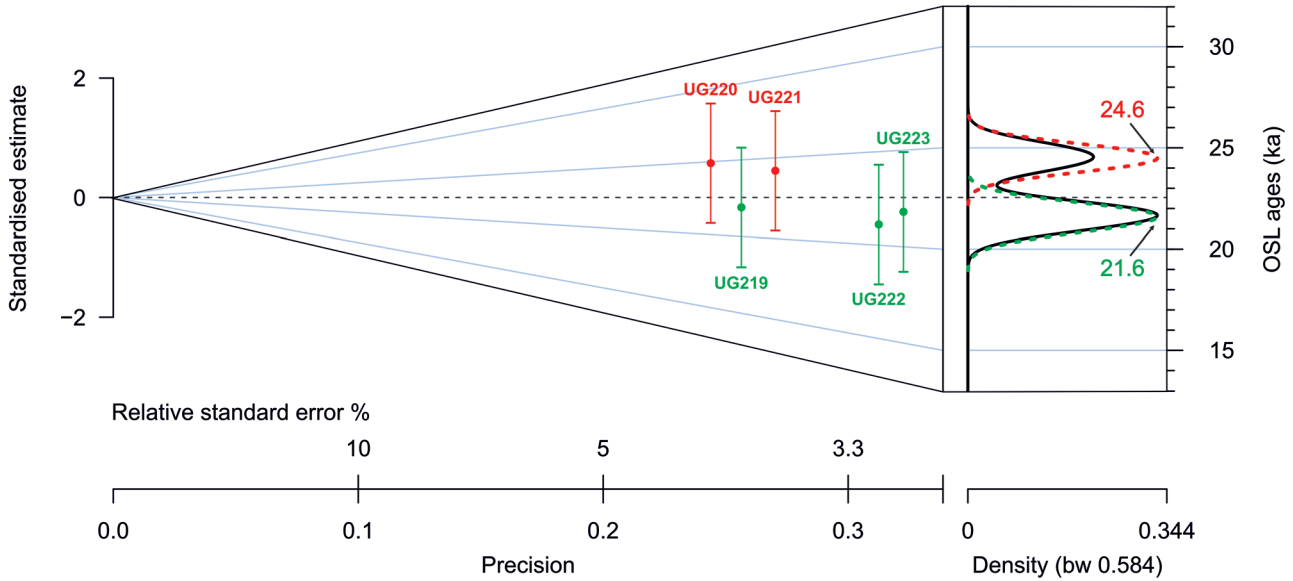
Fig. 7 OSL age estimation based on abanico plot. Black – based on samples UG219-UG223. Note the bimodal distribution displayed in the kernel density estimate (black solid line). Green – based on samples UG219, UG222 and UG223 regarded as most reliable/adequately bleached. Red – based on samples UG220 and UG221 regarded as affected by incomplete bleaching

discharge and sediment supply as well as sheet-flood events and the incision of erosional channels.

Ages for samples UG219, UG222 and UG223, ranging from 21 ± 3 to 22 ± 4 ka are evaluated to be reliable. Moreover, the mean age of these three samples indicating 21.6 ± 3.4 ka (Fig. 7) is used as an equivalent for the calculated OSL ages in this study.

DISCUSSION

The stratigraphy and deformation history of the JGC must be discussed in the frame of the overall ice-margin fluctuation of the FIS. The area of the island of Rügen was ice-free between the LGM advance (Brandenburgian phase, early MIS 2) and a post-LGM re-advance (Pomeranian phase, MIS 2) of the FIS, as indicated by widespread glacifluvial and glacilacustrine deposits of the lithostratigraphic unit I2 (Panzig 1995; Müller, Obst 2006; Kenzler et al. 2017, 2023; Plonka et al. 2022). Chronological data from the I2 unit outcropping at the cliffs of Jasmund peninsula show that this ice-free episode lasted from 23 ± 2 to 20 ± 2 ka (Kenzler et al. 2017; Kenzler, Hüneke 2019). Since the I2 unit includes the youngest pre-kinematic deposits, both the northern and southern part of the JGC subsequently formed by the post-LGM re-advance (Pomeranian phase, MIS 2) of the FIS (Kenzler et al. 2022), probably induced by surge events of the related ice streams (Gehrmann 2018; Gehrmann, Harding 2018, 2019; Gehrmann et
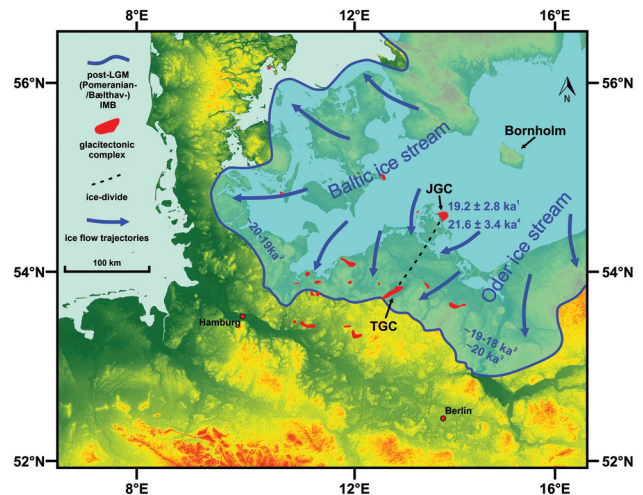
Fig. 8 Overview map showing the maximum extent of the FIS during the MIS 2 post-LGM Pomeranian/Bælthav ice advance. Note the possible ice divide (black dashed line, Tylman et al. 2022) between the JGC and the Teterow Glacitectonic Complex (TGC). Positions of glacitectonic complexes according to Pedersen (2005) and Börner et al. (2019). Cited age data: [1] Kenzler et al. (2023), [2] Tylmann et al. (2022), [3] Hardt, Böse (2016), [4] this study

al. 2022). Finally, the ice overran the study area and reached its maximum position, the Pomeranian IMB (Fig. 8; Litt et al. 2007; Ehlers et al. 2011; Hughes et al. 2016; Tylmann et al. 2022).

A reliable set of age data is now available from pre-kinematic, post-kinematic and, for the first time, syn-kinematic sediments of the JGC (Fig. 9).
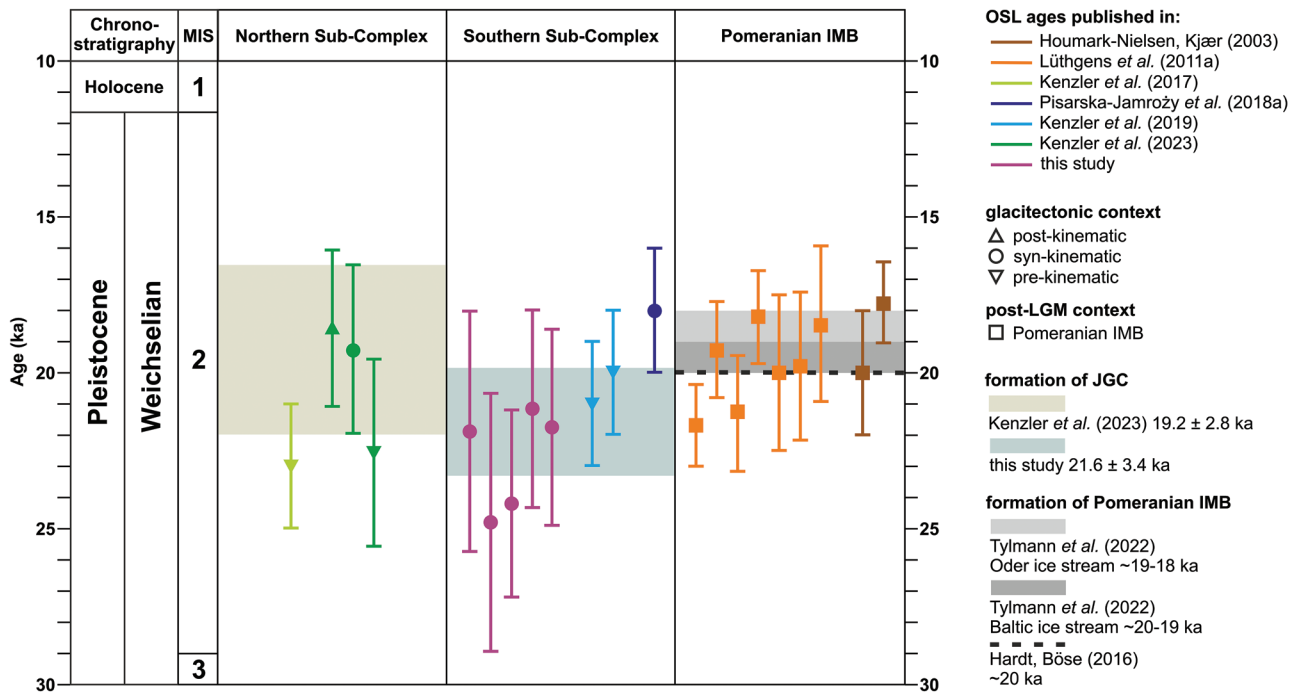
Fig. 9 Age distribution of selected OSL ages for (i) the growth of the northern sub-complex, (ii) the growth of the southern sub-complex and (iii) the Pomeranian IMB (MIS 2). Age estimation of Tylmann *et al.* (2022) based on new and recalculated [10]Be, OSL and radiocarbon ages. Age estimation of Hardt, Böse (2016) based on recalculated [10]Be and OSL ages

Kenzler *et al.* (2022) dated pre-kinematic sediments of the lithostratigraphical unit I1 (Fig. 2) of the northern sub-complex at the Glowe site (Fig. 1B) to be younger than ~ 45–34 ka and concluded that the formation of the JGC occurred subsequently, most probably around 20 ka, incorporating data from prior publications (Steinich 1992; Krbetschek 1995; Kenzler *et al.* 2015, 2017; Pisarska-Jamroży *et al.* 2018a; Kenzler, Hüneke 2019). In addition, Kenzler *et al.* (2023) dated a sedimentary sequence (I2 unit) from a basin structure at the so-called outcrop Stripe 25 of the northern sub-complex (Fig. 1B). The derived OSL ages implicate that the evolution of the northern sub-complex took place during MIS 2 (Kenzler *et al.* 2023). At least one age is obtained from syn-kinematic deposits displaying an age of 19.2 ± 2.8 ka (LUM 3154). Based on this single age and incorporating the statistical error, the evolution of the northern sub-complex took place between 22.0–16.4 ka (Fig. 9). For the formation time of the southern sub-complex, Pisarska-Jamroży *et al.* (2018a) provide an age of 17.9 ± 1.8 ka (LUM 3146) for aeolian sand on top of a glaciofluvial conglomerate (unit A, Fig. 3). According to Plonka *et al.* (2022), the lithological unit A was deposited during a short phase at the beginning of the evolution of the JGC. The lithological log in Pisarska-Jamroży *et al.* (2018a) shows that the sample was taken from a patchy layer with a thickness of ~ 30 cm between a massive conglomerate below and a silty to clayey layer above. An influence by radiation from adjacent layers and rocks on the absorbed dose

rate of the sample cannot be excluded and might led to an underestimation of the true burial dose (Preusser *et al.* 2008; Riedesehl, Autzen 2020; Murray *et al.* 2021). Finally, the new age data presented in this study indicating an age of 21.6 ± 3.4 ka exclusively derived from syn-kinematic deposits, complements the previously published data.

The two-stage main evolution of the JGC is concluded from geomorphological and structural data (Gehrmann 2018; Gehrmann, Harding 2018, 2019; Gehrmann *et al.* 2022). Based on the present data, there is no clear age difference between the OSL data of Kenzler *et al.* (2023) and this study, with 19.2 ± 2.8 ka for the northern and 21.6 ± 3.4 ka for the southern part (Fig. 9). The overlap of the statistical error indicates, on the contrary, the conclusion that both sub-complexes arose penecontemporaneously. It is assumed that the two main evolutional stages took place in a period which is smaller than the statistical error of at least ± 10% characteristic of OSL dating equating to more than ~ 2 ka. Hence, the distinction between the growth of the northern and the southern sub-complex by OSL dating is not conclusive.

The structural two-phase model of the JGC, with ice advancing from different directions (NE, SE), forming the northern and the southern sub-complex as the main evolutional stages during MIS 2 (Gehrmann, Harding 2018, 2019), is in agreement with the asynchronous dynamics of the FIS described by Tylmann *et al.* (2022) for the post-LGM Pomeranian IMB. The latter authors depict the area of Rügen as a

centre of a possible ice divide between the Baltic ice stream (causing the northern sub-complex) and the Oder ice stream (causing the southern sub-complex) (Fig. 8). Based on a compilation of new and recalculated [10]Be surface exposure ages, OSL and radiocarbon ages, Tylmann *et al.* (2022) suggest ages around 20–19 ka for the Baltic ice stream and 19–18 ka for the Oder ice stream reaching its maximum extent. In agreement with these results, we suppose a short-scale temporal offset < 2 ka of both ice streams compared to the model of Lüthgens *et al.* (2020), which concluded that an early MIS 3 ice advance formed the northern part of the JGC, whereas the formation of the southern part is related to a late MIS 3 ice advance. This model implicates an offset of at least 16 ka, which contradicts the existing and presented age data from the Jasmund peninsula. The model of Tylmann *et al.* (2022) is, from a spatial point of view, an analogue to the model of Lüthgens *et al.* (2020) for late MIS 3, which depicts Klintholm and Oder lobes divided by the island of Bornholm (Figs 1A, 8). Both models imply that the island of Bornholm and the Jasmund area, together with the Rønne Bank as a line of elevations in the Baltic Sea, strongly affected the ice flow pattern of the FIS, for the LGM and post-LGM advances of the Weichselian glaciation.

Ludwig (2011) already proposed the occurrence of two ice streams generating the glacitectonic deformation at the Jasmund peninsula and progressively leading to the rise of the JGC. We follow this principal thesis and assume that the topography of the Baltic Sea basin and especially the area of the Jasmund peninsula act as a nunatak, which splits the advancing FIS into two branches giving way to the Baltic and the Oder ice stream.

Apart from the Jasmund peninsula, numerical age data for the German sector of the SW Baltic Sea area is scarce (Hughes *et al.* 2016; Tylmann *et al.* 2022). Regarding the geomorphological record of the Pomeranian IMB in Mecklenburg-Western Pomerania, the assumption about a continuous IMB expanding the whole area existed for a long time (Fig. 8). If there are two separated ice streams, more distinct lobate structures of the IMB would be expected. A hint to a more lobate structure of the ice margin during this time might be the Teterow Glacitectonic Complex (TGC) of the Mecklenburger Schweiz (Nagel, Rühberg 2003; Börner *et al.* 2012, 2019), which is situated in the prolongation on the Bornholm-Rügen ice divide (Tylmann *et al.* 2022) at the intersection of two end-moraine lobes (Fig. 8). The orientation of the TGC lies orthogonal to most of other glacitectonic complexes in the area of Mecklenburg-Western Pomerania, which are normally aligned to the ice marginal positions marked by terminal moraines (Fig. 8). Hence, the TGC might mark the point where the tongues of the Baltic and the Oder ice stream converged. In this area, further dating is of key importance for a better understanding of the regional dynamics of the ice sheet during this period.

With a reliable age of 21.6 ± 3.4 ka for the ice marginal glacitectonic imbrication on the southern sub-complex of the JGC, the OSL data presented in this study pre-date the age assessment of the Pomeranian IMB of Hardt and Böse (2016) and Tylmann *et al.* (2022). These authors suggest ages of 20–18 ka for the formation of the Pomeranian IMB (MIS 2) extent of the FIS in NE Germany (Figs 8, 9). Since Arnold and Sharp (2002) calculated flow velocities of 400 to 600 m/yr for the SW sector of the FIS between 22–18 ka, which roughly equates to 50 km/ka, the difference in age data coincides with the distance between the JGC and the MIS 2 Pomeranian IMB (Fig. 8).

CONCLUSIONS

The syn-kinematic deposits of a piggyback basin infill were tested in order to gain robust age data on the evolution of a glacitectonic complex by means of quartz luminescence dating. As the sediments were deposited proximal to the ice sheet, short transport distances and a large proportion of suspension load may have led to insufficient resetting of the luminescence signal. Nevertheless, the samples analysed in this study yielded reliable ages, using quasi single-grain aliquots (< 1 mm) and statistical models for age calculation.

We conclude that the development of the JGC was triggered by the post-LGM ice advance during MIS 2. The asynchronous advance of the ice margin in the SW Baltic Sea region around the Jasmund peninsula led to the development of distinct ice lobes, which formed the northern (older) and the southern (younger) sub-complex. The evolution of the JGC took place between 22–20 ka. The new OSL data of the Dwasieden cliff section provides an age of 21.6 ± 3.4 ka for the growth of the southern sub-complex. The results of this study (i) are in agreement with the data by Kenzler *et al.* (2023) regarding the evolution of the JGC and (ii) pre-date the NE-Germany maximum extent of the FIS manifesting in the Pomeranian IMB between 20–18 ka (Hardt, Böse 2016; Tylmann *et al.* 2022).

ACKNOWLEDGEMENTS

REFERENCES

Aber, J.S., Ber, A. 2011. Glaciotectonic structures, landforms, and processes. In: Singh, V.P., Singh, P., Haritashya, U.K. (eds). *Encyclopedia of Snow, Ice and Glaciers. Encyclopedia of Earth-Sciences Series.* Springer, Dordrecht, 444–458. DOI 10.1007/978-90-481-2642-2_655

Andrén, T., Björck, S., Andrén, E., Conley, D., Zillén, L., Anjar, J. 2011. The development of the Baltic Sea basin during the last 130 ka. In: Harff, J., Björck, S., Hoth, P. (eds). *The Baltic Sea Basin. Central and Eastern European Development Studies (CEEDES)*, 75–97. DOI 10.1007/978-3-642-17220-5_4

Arnold, L.J., Roberts, R.G. 2009. Stochastic modelling of multi-grain equivalent dose (D$_e$) distributions: Implications for OSL dating of sediment mixtures. *Quaternary Geochronolgy 4 (3)*, 204–230. DOI 10.1016/j.quageo.2008.12.001

Arnold, N., Sharp, M. 2002. Flow variability in the Scandinavian ice sheet: modelling the coupling between ice sheet flow and hydrology. *Quaternary Science Reviews 21*, 485–502. DOI 10.1016/S0277-3791(01)00059-2

Benn, D.I., Evans, D.J.A. 2010. *Glaciers and Glaciations*. London, Hodder Education, 802 pp. DOI 10.1111/j.1502-3885.2011.00212.x

Börner, A., Janke, W., Lorenz, S., Pisarska-Jamroży, M., Rother, H. 2012. Das Jungquartär im Binnenland Mecklenburg-Vorpommerns – glaziale Morphologie, Gewässernetzentwicklung und holozäne Landnutzungsgeschichte [The early Quaternary in the inlandof Mecklenburg-Western Pomerania – glacialmorphology, hydrograpphy and history of holocene landuse]. *Jahresberichte und Mitteilungen des Oberrheinischen Geologischen Vereines 94*, 287–313. [In German] DOI 10.1127/jmogv/94/2012/287

Börner, A., Gehrmann, A., Hüneke, H., Kenzler, M., Lorenz, S. 2019. The Quaternary sequence of Mecklenburg-Western Pomerania: areas of specific interest and ongoing investigations. *DEUQUA Special Publications 2*, 1–10. DOI 10.5194/deuquasp-2-1-2019

Bøtter-Jensen, L., Thomsen, K.J., Jain, M. 2010. Review of optically stimulated luminescence (OSL) instrumental developments for retrospective dosimetry. *Radiation Measurements 45*, 253–257. DOI 10.1016/j.radmeas.2009.11.030

Brumme, J. 2015. Three-dimensional microfabric analyses of Pleistocene tills from the cliff section Dwasieden on Rügen (Baltic Sea coast): micromorphological evidence for subglacial polyphase deformation. *University Greifswald*, PhD thesis, 250 pp.

Brumme, J., Hüneke, H., Phillips, E.R. 2019. Micromorphology and clast microfabrics of subglacial traction tills at the sea cliff Dwasieden: evidence of polyphase syn- and post-depositional deformation. *DEUQUA Special Publications 2*, 51–60. DOI 10.5194/deuquasp-2-51-2019

Cohen, K.M., Gibbard, P.L. 2011. Regional chronostratigraphical correlation table for the last 270,000 years. North Atlantic – Greenland – West, North, Central, Eastern Europe, Russia – Siberia. *INQUA congress pre-edition*. http://posters.geo.uu.nl/2011/COHEN-GIBBARD-270000-yr-ChronoChart-INQUA-2011.pdf

Cohen, K.M., Finney, S.C., Gibbard, P.L., Fan, J.X. 2013. The ICS International Chronostratigraphic Chart. *Episodes 36*, 199–204. DOI 10.18814/EPIIUGS/2013/V36I3/002

Credner, R. 1893. Rügen – Eine Inselstudie [Rügen – study of an island]. *Forschungen zur deutschen Landes- und Volkskunde 7*, 373–494. [in German].

Cunningham, A.C., Wallinga, J. 2010. Selection of integration time intervals for quartz OSL decay curves. *Quaternary Geochronology 5*, 657–666. DOI 10.1016/j.quageo.2010.08.004

Cunningham, A.C., Wallinga, J. 2012. Realizing the potential of fluvial archives using robust OSL chronologies. *Quaternary Geochronology 12*, 98–106. DOI 10.1016/j.quageo.2012.05.007

Cunningham, A.C., Wallinga, J., Minderhoud, P.S.J. 2011. Expectations of scatter in equivalent-dose distributions when using multi-grain aliquots for OSL dating. *Geochronometria 38*, 424–431. DOI 10.2478/s13386-011-0048-z

Duller, G.A.T. 2003. Distinguishing quartz and feldspar in single-grain luminescence measurements. *Radiation Measurements 37*, 161–165. DOI 10.1016/S1350-4487(02)00170-1

Duller, G.A.T. 2008. Single-grain optical dating of Quaternary sediments: why aliquot size matters in luminescence dating. *Boreas 37*, 589–612. DOI 10.1111/j.1502-3885.2008.00051.x

Ehlers, J., Gibbard, P.L., Hughes, P.D. 2011. Quaternary glaciations – extent and chronology. Elsevier, 1126 pp.

Fuchs, M., Woda, C., Bürkert, A. 2007. Chronostratigraphy of a sedimentary record from the Hajar mountain range in north Oman: Implications for optical dating of insufficiently bleached sediments. *Quaternary Geochronology 2*, 202–207. DOI 10.1016/j.quageo.2006.03.006

Fuchs, M., Owen, L.A. 2008. Luminescence dating of glacial and associated sediments: review, recommendations and future directions. *Boreas 37*, 636–659. DOI 10.1111/j.1502-3885.2008.00052.x

Galbraith, R.F., Roberts, R.G., Laslett, G.M., Yoshida, H., Olley, J.M. 1999. Optical dating of single and multiple grains of quartz from Jinmium Rock Shelter, Northern Australia: part I, experimental design and statistical models. *Archaeometry 41*, 339–364. DOI 10.1111/j.1475-4754.1999.tb00987.x.

Gehrmann, A. 2018. The multi-stage structural development of the Upper Weichselian Jasmund Glactectonic Complex (Rügen, NE Germany). *University of Greifswald*, PhD thesis, 278 pp.

Gehrmann, A., Harding, C. 2018. Geomorphological mapping and spatial analyses of an Upper Weichselian

glacitectonic complex based on LiDAR data, Jasmund peninsula (NE Rügen), Germany. *Geosciences 8*, 1–24. DOI 10.3390/geosciences8060208

Gehrmann, A., Harding, C. 2019. Blieschow on Jasmund – geomorphology and glacigenic landforms: keys to understanding the deformation chronology of Jasmund. In: *DEUQUA Special Publications 2*, 11–17. DOI 10.5194/deuquasp-2-11-2019

Gehrmann, A., Hüneke, H., Meschede, M., Phillips, E.R. 2017. 3D microstructural architecture of deformed glacigenic sediments associated with large-scale glacitectonism, Jasmund Peninsula (NE Rügen), Germany. *Journal of Quaternary Science 32 (2)*, 213–230. DOI 10.1002/jqs.2843

Gehrmann, A., Pedersen, S.A.S., Meschede, M. 2022. New insights into the structural development and shortening of the southern Jasmund glacitectonic complex (Rügen, Germany) based on balanced cross sections. *International Journal of Earth Sciences 111*, 1697–1715. DOI 10.1007/s00531-022-02216-y

Groth, K. 2003. Zur glazitektonischen Entwicklung der Stauchmoräne Jasmund/Rügen [On the glacitectonic evolution of the Jasmund push moraine, Rügen]. *Schriftenreihe des Landesamtes für Umwelt, Naturschutz und Geologie Mecklenburg-Vorpommern 3*, 39–49. [In German].

Guerin, G., Mercier, N., Adamiec, G. 2011. Dose-rate conversion factors: update. *Ancient TL 29*, 5–8.

Hardt, J., Böse, M. 2016. The timing of the Weichselian Pomeranian ice marginal position south of the Baltic Sea: a critical review of morphological and geochronological results. *Quaternary International 478*, 51–58. DOI 10.1016/j.quaint.2016.07.044

Hardt, J., Lüthgens, C., Hebenstreit, R., Böse, M. 2016. Geochronological (OSL) and geomorphological investigations at the presumed Frankfurt ice marginal position in northeast Germany. *Quaternary Science Reviews* 154, 85–99. DOI 10.1016/j.quascirev.2016.10.015

Houmark-Nielsen, M. 2010. Extent, age and dynamics of Marine Isotope Stage 3 glaciations in the southwestern Baltic Basin. *Boreas 39*, 343–359. DOI 10.1111/j.1502-3885.2009.00136.x

Houmark-Nielsen, M., Kjær, K.H. 2003. Southwest Scandinavia, 40–15 ka BP: palaeogeography and environmental change. *Journal of Quaternary Science 18*, 769–786. DOI 10.1002/jqs.802

Hughes, A.L.C., Gyllencreutz, R., Lohne, Ø.S., Mangerud, J., Svendsen, J.I. 2016. The last Eurasian ice sheet-a chronological database and time-slice reconstruction, DATED-1. *Boreas 45*, 1–45. DOI 10.1111/bor.12142

Jaekel, O. 1917. Neue Beiträge zur Tektonik des Rügener Steilufers [New contribution to the tectonics of the Rügen cliff]. *Zeitschrift der Deutschen Geologischen Gesellschaft 69*, 81–176. [In German].

Keilhack, K. 1912. Die Lagerungsverhältnisse des Diluviums in der Steilküste von Jasmund auf Rügen [The stratigraphic conditions of the Diluvium at the cliff of Jasmund/Rügen]. *Jahrbuch der preußischen geologischen Landesanstalt 33*, 114–158. [In German].

Kenzler, M., Hüneke, H. 2019. Sea cliff at Glowe: stratigraphy and absolute age chronology of the Jasmund Pleistocene sedimentary record. *DEUQUA Special Publications 2*, 43–50. DOI 10.5194/deuquasp-2-43-2019

Kenzler, M., Obst, K., Hüneke, H., Schütze, K. 2010. Glazitektonische Deformation der kretazischen und pleistozänen Sedimente an der Steilküste von Jasmund nördlich des Königsstuhls, Rügen [Glacitectonic deformation of Cretaceous and Pleistocene sediments at the Jasmund cliff north of the Königsstuhl, Rügen]. *Brandenburger Geowissenschaftliche Beiträge 17*, 107–122. [In German].

Kenzler, M., Tsukamoto, S., Meng, S., Thiel, C., Frechen, M., Hüneke, H. 2015. Luminescence dating of Weichselian interstadial sediments from the German Baltic Sea coast. *Quaternary Geochronology 30*, 215–256. DOI 10.1016/j.quageo.2015.05.015

Kenzler, M., Tsukamoto, S., Meng, S., Frechen, M., Hüneke, H. 2017. New age constraints from the SW Baltic Sea area – implications for Scandinavian Ice Sheet dynamics and palaeoenvironmental conditions during MIS 3 and early MIS 2. *Boreas 46 (1)*, 34–52. DOI 10.1111/bor.12206

Kenzler, M., Krauß, N., Hüneke, H. 2022. Testing a proposed new chronology for the Jasmund Glacitectonic complex (SW Baltic Sea): no indication of incipient deformation during MIS 3. *Quaternary Geochronology 70*, 101299. DOI j.quageo.2022.101299

Kenzler, M., Gibb, M.A., Gehrmann, A., Deutschmann, A., Rother, H., Obst, K., Hüneke, H. 2023. Identification of Quaternary alluvial-fan deposits (Rügen, SW Baltic Sea): Significance for recognition of syn-kinematic sedimentation in glacitectonic complexes. *Geomorphology 424*, 108558. DOI j.geomorph.2022.108558

Kleman, J., Hättestrand, M., Borgström, I., Fabel, D., Preusser, F. 2021. Age and duration of a MIS 3 interstadial in the Fennoscandian Ice Sheet core area – Implications for ice sheet dynamics. *Quaternary Science Reviews 264*, 107011. DOI j.quascirev.2021.107011

Krbetschek, M.R. 1995. Lumineszenz-Datierungenquartärer Sedimente Mittel-, Ost- und Nordostdeutschlands [Luminescence dating of quaternary sediments from Middle-, East- and Nordeastern Germany]. *TU Bergakademie Freiberg*, PhD thesis, 122 pp. [In German].

Kreutzer, S., Burow, C., Dietze, M., Fuchs, M.C., Schmidt, C., Fischer, M., Friedrich, J., Mercier, N., Smedley, R.K., Christophe, C., Zink, A., Durcan, J., King, G.E., Philipp, A., Guerin, G., Riedesel, S., Autzen, M., Guibert, P., Mittelstrass, D., Gray, H.J., Fuchs, M. 2020. *Package 'Luminescence' – comprehensive luminescence dating data analysis. R package version 0.9.15*. URL: https://CRAN.R-project.org/package=Luminescence

Lepper, K., McKeever, W.S. 2002. An objective methodology for dose distribution analysis. *Radiation Protection Dosimetry 101 (1–4)*, 349–352. DOI 10.1093/oxfordjournals.rpd.a005999

Litt, T., Behre, K.E., Meyer, K.D., Stephan, H.J., Wansa, S. 2007. Stratigraphische Begriffe für das Quartär

des norddeutschen Vereisungsgebietes [Stratigraphical terms for the Quaternary of the North German Glaciation Area]. In: Litt, T. (ed.) *Stratigraphie von Deutschland – Quartär. E&G Quaternary Science Journal 56 (1/2),* 7–65. [In German].

Ludwig, A.O. 2011. Zwei markante Stauchmoränen: Peski/Belorussland und Jasmund, Ostseeinsel Rügen/Nordostdeutschland – Gemeinsame Merkmale und Unterschiede [Two striking push moraines: Peski/Belorussland and Jasmund/Rügen Island, NE Germany – common features and differences]. *E&G Quaternary Science Journal 60 (4),* 464–487. [In German]. DOI 10.3285/eg.60.4.06

Lüthgens, C., Böse, M., Krbetschek, M. 2010a. On the age of the young morainic morphology in the area ascribed to the maximum extent of the Weichselian glaciation in north-eastern Germany. *Quaternary International 222,* 72–79. DOI 10.1016/j.quaint.2009.06.028

Lüthgens, C., Krbetschek, M., Böse, M., Fuchs, M.C. 2010b. Optically stimulated luminescence dating of fluvioglacial (sandur) sediments from north-eastern Germany. *Quaternary Geochronology 5,* 237–243. DOI 10.1016/j.quageo.2009.06.007

Lüthgens, C., Böse, M., Lauer, T., Krbetschek, M., Strahl, J., Wenske, D. 2011a. Timing of the last interglacial in northern Europe derived from optically stimulated luminescence (OSL) dating of a terrestrial Saalian-Eemian-Weichselian sedimentary sequence in NE-Germany. *Quaternary International 241,* 79–96. DOI 10.1016/j.quaint.2010.06.026

Lüthgens, C., Böse, M., Preusser, F. 2011b. Age of the Pomeranian ice marginal position in northeastern Germany determined by Optically Stimulated Luminescence (OSL) dating of glaciofluvial sediments. *Boreas 40,* 598–615. DOI 10.1111/j.1502-3885.2011.00211.x

Lüthgens, C., Hardt, J., Böse, M. 2020. Proposing a new conceptual model for the reconstruction of ice dynamics in the SW sector of the Scandinavian Ice Sheet (SIS) based on the reinterpretation of published data and new evidence from optically stimulated luminescence (OSL) dating. *E&G Quaternary Science Journal 69,* 201–223. DOI 10.5194/egqsj-69-201-2020

Marks, L. 2012. Timing of the Late Vistulian (Weichselian) glacial phases in Poland. *Quaternary Science Reviews 44,* 81–88. DOI 10.1016/j.quascirev.2010.08.008

Miall, A.D. 1996. The Geology of Fluvial Deposits: Sedimentary Facies, Basin Analysis, and Petroleum Geology. New York: Springer, 582 pp. DOI 10.1007/978-3-662-03237-4

Müller, U., Obst, K. 2006. Lithostratigraphy and bedding of the Pleistocene deposits in the area of Lohme (Jasmund/Rügen). *Zeitschrift der Geologischen Wissenschaften 34,* 39–54.

Murray, A.S., Wintle, A.G. 2000. Luminescence dating of quartz using an improved single-aliquot regenerative-dose protocol. *Radiation Measurements 32,* 57–73. DOI 10.1016/S1350-4487(99)00253-X

Murray, A.S., Olley, J.M., Caitcheon, G. 1995. Measurement of equivalent doses in quartz from contemporary water-lain sediments using optically stimulated luminescence. *Quaternary Science Reviews 14,* 365–371. DOI 10.1016/0277-3791(95)00030-5

Murray, A.S., Thomsen, K.J., Masuda, N., Buylaert, J.P., Jain, M. 2012. Identifying well-bleached quartz using the different bleaching rates of quartz and feldspar luminescence signals. *Radiation Measurements 47,* 688–695. DOI 10.1016/j.radmeas.2012.05.006

Murray, A.S., Arnold, L.J., Buylaert, J.P., Guérin, G., Qin, J., Singhvi, A.K., Smedley, R., Thomsen, K.J. 2021. Optically stimulated luminescence dating using quartz. *Nature Reviews Methods Primers 1 (1).* DOI 10.1038/s43586-021-00068-5

Nagel, D., Rühberg, N. 2003. Naturpark „Mecklenburgische Schweiz und Kummerower See" – quartärgeologische Entstehung einer Landschaft [Nature park „Mecklenburgische Schweiz and Kummerower See" – geological genesis of a landscape during Quaternary]. *Neubrandenburger Geologische Beiträge 3,* 49–62. [In German].

Niedermeyer, R.O., Kanter, L., Kenzler, M., Panzig, W.A., Krienke, K., Ludwig, A.O., Schnick, H.H., Schütze, K. 2010. Rügen Island (I) – Facies, stratigraphy, structural architecture and geological hazard potential of Pleistocene deposits of the Jasmund cliff coast. In: Lampe, R., Lorenz, S. (eds), *Eiszeitlandschaften in Mecklenburg-Vorpommern. Geozon Science Media,* Greifswald, 50–71.

Olley, J., Caitcheon, G., Roberts, R. 1999. The origin of dose distributions in fluvial sediments, and the prospect of dating single grains from fluvial deposits using optically stimulated luminescence. *Radiation Measurements 30,* 207–217. DOI 10.1016/S1350-4487(99)00040-2

Panzig, W.A. 1995. Zum Pleistozän von Rügen [The Pleistocene of Rügen]. *Terra Nostra 6,* 177–200. [In German].

Pedersen, S.A.S. 2005. Structural analysis of the Rubjerg-Knude Glaciotectonic complex Vendsyssel, northern Denmark. *Geological Survey of Denmark and Greenland Bulletin 8,* 192. DOI 10.34194/geusb.v8.5253

Pedersen, S.A.S. 2014. Architecture of Glaciotectonic Complexes. *Geosciences 4,* 269–296. DOI 10.3390/geosciences4040269

Pedersen, S.A.S., Gravesen, P. 2006. Geological Map of Denmark, 1:50,000, Møn. *Geological Survey of Denmark and Greenland Bulletin 28,* 29–32. DOI 10.34194/geusb.v28.4714

Pedersen, S.A.S., Gravesen, P. 2009. Structural development of Maglevandsfald: a key to understanding the glaciotectonic architecture of Møns Klint. *Geological Survey of Denmark and Greenland Bulletin 17,* 29–32. DOI 10.34194/geusb.v17.5007

Pisarska-Jamrozy, M.G., Belzyt, S., Börner, A., Hoffmann, G., Hüneke, H., Kenzler, M., Obst, K., Rother, H., Van Loon, A.J. 2018a. Evidence for glacio-isostatically induced crustal faulting in front of an advancing land-

ice mass (Rügen Island, NE Germany). *Tectonophysics 745*, 338–348. DOI 10.1016/j.tecto.2018.08.004

Pisarska-Jamrozy, M.G., Van Loon, A.J., Bronikowska, M. 2018b. Dump stones as records of overturning ice rafts in a Weichselian proglacial lake (Rügen Island, NE Germany). *Geological Quarterly 62 (4)*, 917–924. DOI 10.7306/gq.1448

Pisarska-Jamrozy, M.G., Belzyt, S., Börner, A., Hoffmann, G., Hüneke, H., Kenzler, M., Obst, K., Rother, H., Steffen, H., Steffen, R., Van Loon, A.J. 2019. The sea cliff at Dwasieden: soft-sediment deformation structures triggered by glacial isostatic adjustment in front of the advancing Scandinavian Ice Sheet. *DEUQUA Special Publications 2*, 61–67. DOI 10.5194/deuquasp-2-61-2019

Plonka, N., Kenzler, M., Hüneke, H. 2022. Syn-kinematic sedimentation between ice margin-parallel thrust-bounded ridges of the glacitectonic complex of Jasmund (Rügen Island, SW Baltic Sea, Weichselian). *Quaternary International 630*, 48–64. DOI 10.1016/j.quaint.2021.02.040

Prescott, J.R., Stephan, L.G. 1982. The contribution of cosmic radiation to the environmental dose for thermoluminescence dating – Latitude, altitude and depth dependences. *PACT 6*, 17–25.

Prescott, J.R., Hutton, J.T. 1994. Cosmic ray contributions to dose rates for luminescence and ESR dating: large depths and long-term variations. *Radiation Measurements 23*, 497–500. DOI 10.1016/1350-4487(94)90086-8

Preusser, F., Degering, D., Fuchs, M., Hilgers, A., Kadereit, A., Klasen, N., Krbetschek, M., Richter, D., Spencer, J.Q.G. 2008. Luminescence dating: basics, methods and applications. *E&G Quaternary Science Journal 57/1–2*, 95–149. DOI 10.23689/fidgeo-1272

Riedesehl, S., Autzen, M. 2020. Beta and gamma dose rate attenuation in rocks and sediment. *Radiation Measurements 133*, 106295. DOI 10.1016/j.radmeas.2020.106295

Roberts, R.G., Galbraith, R.F., Yoshida, H., Laslett, G.M., Olley, J.M. 2000. Distinguishing dose populations in sediment mixtures: a test of single-grain optical dating procedures using mixtures of laboratory-dosed quartz. *Radiation Measurements 32*, 459–465. DOI 10.1016/S1350-4487(00)00104-9

Rodnight, H. 2008. How many equivalent dose values are needed to obtain a reproducible distribution? *Ancient TL 26 (1),* 3–9.

Shen, H.Y., Yu, L.P., Zhang, H.M., Zhao, M., Lai, Z.P. 2015. OSL and radiocarbon dating of flood deposits and its paleoclimatic and archaeological implications in the Yihe River Basin, East China. *Quaternary Geochronology 30*, 398–404. DOI 10.1016/j.quageo.2015.03.005

Steinich, G. 1992. Die stratigraphische Einordnung der Rügen-Warmzeit [The stratigraphical classification of the Rügen warm period]. *Zeitschrift für geologische Wissenschaften 20*, 125–154. [In German].

Thrasher, I.M., Mauz, B., Chiverrell, R.C., Lang, A. 2009. Luminescence dating of glaciofluvial deposits: A review. *Earth-Science Reviews 97*, 133–146. DOI 10.1016/j.earscirev.2009.09.001

Tylmann, K., Rinterknecht, V.R., Wozniak, P.P., Guillou, V., ASTER Team. 2022. Asynchronous dynamics of the last Scandinavian Ice Sheet along the Pomeranian ice marginal belt: A new scenario inferred from surface exposure [10]Be dating. *Quaternary Science Reviews 294*, 1–17. DOI 10.1016/j.quascirev.2022.107755

Van der Wateren, F.M. 1986. Structural geology and sedimentology of the Dammer Berge push moraine. In: Van der Meer, J.J.M. (ed.) *Tills and Glaciotectonics*. Balkema, Rotterdam, 157–182.

Winsemann, J., Koopmann, H., Tanner, H.C., Lutz, R., Lang, J., Brandes, C., Gaedicke, C. 2020. Seismic interpretation and structural restoration of the Heligoland glaciotectonic thrust-fault complex: Implications for multiple deformation during (pre-) Elsterian to Warthian ice advances into the southern North Sea Basin. *Quaternary Science Reviews 227*, 106068. DOI 10.1016/j.quascirev.2019.106068

Wintle, A.G., Murray, A.S. 2006. A review of quartz optically stimulated luminescence characteristics and their relevance in single-aliquot regeneration dating protocols. *Radiation Measurements 41*, 369–391. DOI 10.1016/j.radmeas.2005.11.001